Spectrochimica Acta Part A: Molecular and Biomolecular Spectroscopy 311 (2024) 123983

Contents lists available at ScienceDirect

Spectrochimica Acta Part A:
Molecular and Biomolecular Spectroscopy

journal homepage: www.journals.elsevier.com/spectrochimica-acta-part-a-molecular-and-biomolecular-spectroscopy

A stable and sensitive 2D SERS sensor for bioanalytical applications

Marianna Pannico *, Pellegrino Musto *

National Research Council of Italy, Institute for Polymers, Composites and Biomaterials, 80078 Pozzuoli (NA), Italy

HIGHLIGHTS

- A sensitive and stable SERS sensor based on gold nanospheres deposition.
- SEM and AFM analysis of the sensor surface highlights optimum surface morphology.
- High SERS activity: Enhancement Factor = 2.3×10^8.
- Well suited for the Therapeutic Drug Monitoring of anticancer agents.
- Reliable quantitative analysis in a concentration range of clinical interest.

GRAPHICAL ABSTRACT

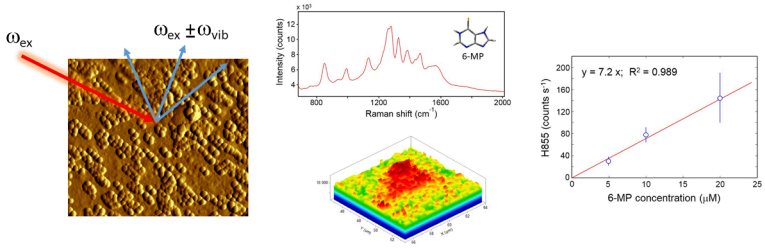

ARTICLE INFO

Keywords:
SERS
Raman imaging
AFM
Therapeutic Drug Monitoring
6-mercaptopurine

ABSTRACT

In this study, we describe a 2D-SERS sensor obtained by deposition of spherical gold nanoparticles (AuNPs) onto a suitably functionalized metal surface. Morphological analysis of the SERS surface by SEM and AFM demonstrated a uniform and stable distribution of the active nanoparticles. Following p-mercaptoaniline (pMA) functionalization, the sensor was characterized by co-localized Raman measurements, demonstrating a significant enhancement in Raman signals with homogeneous SERS activity across the entire sampled area. The as-prepared SERS sensor was demonstrated to be suitable for Therapeutic Drug Monitoring (TDM) of 6-mercaptopurine (6-MP), exhibiting a linear correlation between analyte concentration and SERS intensity in the range 5 – 20 μM. This work highlights the potential of 2D-SERS sensors for hypersensitive and accurate analytical measurements, particularly in the biomedical field.

1. Introduction

In the past few decades, surface enhanced Raman scattering (SERS) has emerged as a powerful analytical technique due to its high sensitivity and fingerprinting character [1–3]. SERS has been widely applied in several fields including food safety, environmental monitoring, biomedicine and analytical chemistry [2,4–6]. Several methods have been employed to fabricate active SERS substrates with specific characteristics: high analytical Enhancement Factor (*EF*), point-to-point repeatability and sample-to-sample reproducibility, stability on storage, and low cost [4,6–8]. Noble metals nanoparticles (AuNPs, AgNPs) with different sizes and shapes represent active and versatile SERS platforms that can be used in two ways: in aqueous colloidal solutions (3D substrates) or deposited on suitably treated solid substrates (2D substrates). For analytical applications, colloidal solutions offer the advantages of stability and spatially uniform response, sometimes at the cost of a reduced sensitivity due to the dilution effect. Furthermore, the signal intensity in solution can be affected by factors such as

* Corresponding authors.
E-mail addresses: marianna.pannico@ipcb.cnr.it (M. Pannico), pellegrino.musto@cnr.it (P. Musto).

https://doi.org/10.1016/j.saa.2024.123983
Received 4 December 2023; Received in revised form 23 January 2024; Accepted 29 January 2024
Available online 1 February 2024

aggregation, precipitation and analyte adsorption kinetics that must be carefully controlled to get a reproducible response [3,6].

In our previous works colloidal AuNPs were demonstrated to be a stable SERS platform that might be used in the clinical practice of Therapeutic Drug Monitoring (TDM). TDM consists in monitoring continuously the drug concentration in biological fluids (most commonly, plasma, serum and/or urine) in order to establish a dosing schedule that would maximize therapeutic results and minimize toxicity [9,10]. The AuNPs were tested as SERS sensor for the detection of the anticancer drug 6-MP, which is one of the most widely used chemotherapeutic agents, mainly employed as immunosuppressant and in the treatment of acute lymphoblastic leukemia [11]. Current analytical methods for TDM are Gas Chromatography/Mass Spectrometry (GC–MS) and Liquid Chromatography coupled with tandem Mass Spectrometry (HPLC-MS/MS) [12,13]. These reference methods represent the gold standard for TDM but the analyses are costly and require highly trained personnel and expensive infrastructures. Alternative analytical methods for TDM capable to provide a rapid and reliable response with less demanding resources and simpler protocols are highly required.

In the first contribution from our group the response function of the 3D-sensor was found to be highly linear with concentration in a range between 1 and 20 μM (the blood concentrations of clinical interest [14]; in this interval an accurate and reproducible quantitative analysis is feasible [15]. In the second paper we improved the sensitivity of the colloidal SERS platform by adjusting the solution pH and inducing a controlled aggregation of the AuNPs (the limit of detection improved from 1.0 to 0.1 μM) but the upper limit of the linearity range decreased to 15 μM [16].

In the present contribution we have investigated a 2D platform fabricated by deposition of AuNPs on a functionalized solid substrate. 2D SERS substrates are expected to provide an increased sensitivity in comparison to colloidal solutions because of the formation of a large number of hot-spots, which strongly enhance the plasmonic effect. The main issues of planar substrates consist in getting a stable and uniform nanoparticle coverage of the active surface and in avoiding fluorescence. Several strategies have been proposed to immobilize nanoparticles on solid substrates [2,6,8]. We describe an approach based on the formation of a self-assembled monolayer (SAM) of a dithiol linker on a metallic surface. The characterization of the derivatized surface before and after AuNPs deposition is presented. The proposed sensor has been investigated in terms of SERS activity, stability and response consistency using a classical SERS probe (pMA); finally, the analytical application to the detection of 6-MP is discussed.

2. Experimental

2.1. Materials

Trisodium citrate (TC), gold (III) chloride trihydrate ($HAuCl_4{\cdot}3H_2O$), ascorbic acid (AA), sodium borohydride ($NaBH_4$), Cetyltrimethylammonium bromide (CTAB), ethanol, methanol, p-Mercaptoaniline (pMA), 1,4-Butanedithiol (BDT), 6-mercaptopurine (6-MP) and gold coated glass cover slip 22×22 mm (Au layer thickness 100 Å) were purchased from Sigma-Aldich. Milli-Q water was used for the preparation of gold nanoparticles.

2.2. Synthesis and surface functionalization of gold nanoparticles

The AuNPs were synthesized in aqueous solution by using the seed-mediated growth method as described in our previous work [17]. Once prepared, the AuNPs solution was stirred for 10 min and then centrifuged three times at 13,000 rpm at 35 °C for 20 min. The AuNPs were re-suspended in water and kept at room temperature for further characterization.

The SERS performance of the synthesized AuNPs was evaluated using the enhancement factor (*EF*) as a figure of merit. *EF* was evaluated by comparing the spontaneous and the surface enhanced spectra of pMA according to $EF = (I_{SERS}{\cdot}N_{REF})/(I_{REF}{\cdot}N_{SERS})$ where I_{SERS} is the integrated area of a specific SERS signal (at 1074 cm^{-1}) and I_{REF} is the integrated area of the corresponding Raman signal (at 1088 cm^{-1}), both normalized for exposure time. Analogously, N_{SERS} and N_{REF} represent the number of molecules contributing to the SERS and the Raman signal, respectively, and were evaluated according to the procedure described in refs [17,18].

To this end, an AuNPs colloidal solution was functionalized at room temperature with a 100 μM pMA/ethanol solution, added in a 1:1 vol ratio under continuous magnetic stirring (10 min).

2.3. Preparation of the 2D-SERS platform

To get a stable 2D-SERS platform a commercial gold-coated glass plate 22×22 mm was used as substrate (plain gold substrate, PGS). The PGS was cut in several pieces (~2×2 mm) which were then utilized to prepare different 2D-SERS platforms. First, the PGS surface was washed several times with pure methanol and then functionalized by immersion for five days in a solution of BDT in methanol (PGS@BDT). Several BDT concentrations were tested (1, 2, 4 mM) and contact angle measurements indicated that the optimum result is obtained with a 4 mM concentration [see Fig. S1, Supplementary Information (*SM*)]. The as prepared PGS@BDT substrate was removed from the BDT solution, washed several times with methanol and dried under nitrogen flux. Then, a 15 nM colloidal solution of AuNPs in water was dropped on the PGS@BDT surface and allowed to dry at room temperature under a laminar flux hood. The obtained 2D-SERS platform (PGS@BDT@AuNPs) was thoroughly washed with milliQ water to remove the excess of non-bonded nanoparticles. Several 2D-SERS platforms were produced to test the reproducibility. Moreover, a reference sample (PGS/AuNPs) was prepared using the same procedure without the BDT functionalization step. The surface structure of the resulting 2D-SERS platforms was characterized by Scanning Electron Microscopy (SEM) and atomic force microscopy (AFM). The SERS performance was tested by running Raman measurements in the mapping mode on the SERS substrates functionalized with pMA. Functionalization was achieved by drop-casting a 100 μM pMA/ethanol solution, followed by drying at room temperature. An analytical application of the proposed sensor was tested with 6-MP, one of the most used anticancer agents: a water stock solution of 6-MP (1 mM) was prepared and used to get diluted 6-MP solutions ranging from 5 to 20 μM. The drug solutions were drop-cast on the SERS substrates and after water evaporation co-localized AFM/Raman measurements were run.

2.4. Characterization techniques

2.4.1. UV–VIS spectroscopy

The optical properties of AuNPs and their molar concentration were measured by an UV–VIS spectrophotometer equipped with a single monochromator (V − 570 from Jasco, Easton, USA). Absorption spectra of the AuNPs colloids were collected using a quartz cell with a 1.00 cm path length; the scan speed was 400 nm/min and the wavelength range was 300 to 800 nm.

A set of eight standards were prepared by diluting the synthetized AuNPs solution batch for the quantitative analysis of the gold amount. It was assumed that the reduction from Au(III) to Au(0) was complete.

2.4.2. Transmission electron microscopy

The AuNPs morphology, size and shape, were examined by bright field transmission electron microscopy (TEM) analysis performed on a FEI Tecnai G12 Spirit Twin (LaB6 source) equipped with a FEI Eagle 4 K CCD camera (Eindhoven, The Netherlands) operating with an acceleration voltage of 120 kV. The colloidal solution was deposited by immersion on a carbon-coated copper grid for TEM examination. After

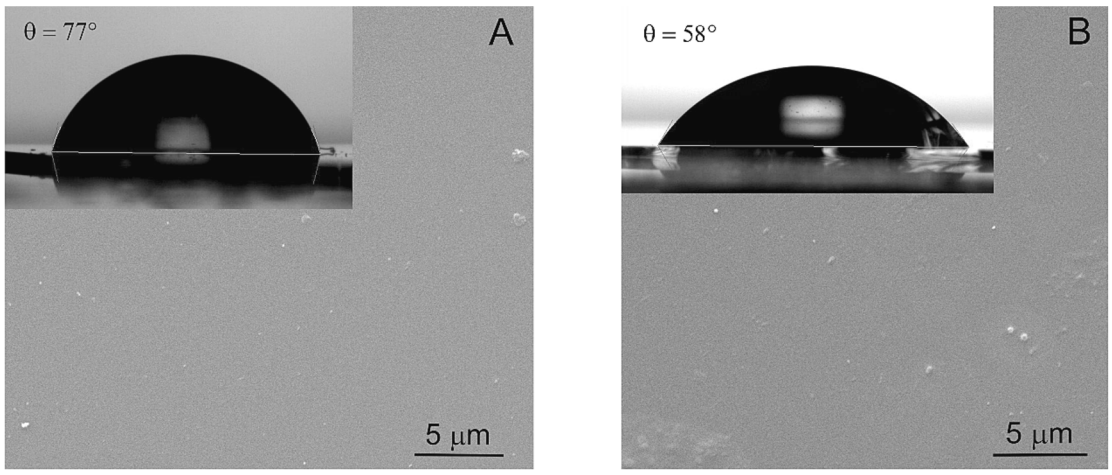

Fig. 1. SEM micrographs and contact angle measurement (insets) for the PGS and the PGS@BDT surfaces (1A and 1B, respectively).

drying TEM images were acquired in different sample areas and were transferred in a standard graphic format (.tif files) to perform an off-line Statistical Image Analysis (SIA) by the PLS/MIA software package, (Eigenvector Research Inc., Manson, WA, USA) running under the MATLAB computational platform (Mathworks, Natick, MA, USA).

2.4.3. Scanning electron microscopy

Morphological characterization of the 2D-SERS surface was performed by Scanning Electron Microscope (SEM) FEI Quanta 200 FEG) with Energy-dispersive X-ray spectroscopy (EDX) (Japan).

2.4.4. Contact angle measurements

The surface wettability of the PGS/BDT substrate was evaluated by measuring the contact angle (θ) by using an optical contact angle device, Drop Shape Instruments FTA1000 (Portsmouth, VA, USA), equipped with a high-resolution video camera (752 × 582 pixels and image acquisition speed equal to 25 frames per second). The static contact angle of water at room temperature (θ, deg) was measured by dropping five drops of deionized water (5 μL) onto the substrate surface. The contact angle (CA) was calculated immediately after droplet deposition by means of the angle between the baseline of the drop and the tangent. An average θ value of five measurements per substrate was reported. The CA of the PGS substrate was similarly measured for comparison.

2.4.5. Atomic force microscopy

Atomic force microscopy (AFM) was used to characterize the morphology of the 2D-SERS platform. AFM measurements were carried out by the OmegaScope AFM instrument (Horiba-Jobin Yvon, Edison, NJ, USA).

AFM images of 10 × 10 μm^2 areas (520 x 520 points) were collected on random places on the surface sample in noncontact mode with an aluminum coated AFM tip NSC14/Al BS with a force constant of 5 N/m (1.8–13 N/m).

AFM measurements were run on the PGS to compare the morphology of the reference sample.

2.4.6. Raman spectroscopy

The Raman spectra were collected by a XploRA Plus confocal Raman micro-spectrometer (Horiba-Jobin Yvon, Edison, NJ, USA) operating with a 638 nm diode laser as exciting source. The 180° back-scattered radiation was collected by an Olympus metallurgical objective (MPlan 10x, NA = 0.28, laser power 25.4 mW) with a 600 grooves/mm grating and confocal and slit apertures set to 500 and 200 μm, respectively. The radiation was focused onto a CCD detector (Syncerity) cooled at −60 °C by a Peltier module. The reference spectrum of pMA was collected on a 10 wt% pMA ethanol solution by using a quartz cuvette with chamber volume of 700 μL (Hellma GmbH & Co, Jena, Germany) and 10 s of acquisition time. The pMA SERS spectrum in the colloidal solution was collected in the same operating conditions. The 6-MP reference spectrum was collected by dropping a 100 μM 6-MP water solution on an aluminum support and after water evaporation. The spectrum was acquired by an Olympus metallurgical objective (MPlan 50x, NA = 0.50) and 10 s of acquisition time.

Co-localized AFM and Raman measurements were run in tip-scanning mode by the Horiba XploRA Plus confocal Raman microspectrometer coupled to the OmegaScope AFM platform by an optical bridge. For the AFM-Raman measurements a silicon tip ACCESS-NC-A-10 (reflex side Al coated) with a spring constant of 78 N/m (25–95 N/m) was used. The 2D-SERS platform was functionalized with 100 μM pMA ethanol solution and after drying, the co-localized topographic maps were collected on an area of 10 × 10 μm^2 with a 0.25 μm step size, MPlan x100 (NA = 0.70) objective and 2 s of acquisition time. Several maps were collected in different regions of the sample. A PGS/AuNPs substrate without BDT functionalization was also tested with the pMA/ethanol solution in the same conditions.

AFM-Raman measurements were run on the 2D-SERS substrate functionalized with 6-MP at different concentration ranging from 5 to 20 μM. The topographic maps were collected in different regions of the samples on an area of 10 × 10 μm with the same operating conditions used for the pMA functionalized 2D-SERS platform.

All the collected Raman data were converted into ASCII format and transferred to the MATLAB computational platform for further processing.

3. Results and discussion

3.1. Morphology

The Statistical Image Analysis performed on the collected TEM micrographs (a total nanoparticles population of ≅ 700 units) is reported in Fig. S2, *SM*. 98 % of the population is characterized by a spherical shape (roundness ≥ 0.85) and an average diameter of 16 nm with a narrow size distribution (Full width at Half maximum, FWHM, = 3.5 nm, which corresponds to a standard deviation of the average diameter of ± 1.5 nm).

The Au molar concentration was estimated by UV–Vis spectroscopy [15] to be 1.84 mM, which corresponds to 15 nM of AuNPs. The spectrum of the gold colloids displays a sharp and symmetrical bandshape peaked at 526 nm, which confirms the narrow distribution of particle sizes (see Fig. S3, *SM*).

The synthesized AuNPs were employed to fabricate a 2D-SERS sensor, after suitable functionalization of the PGS surface. Chemical

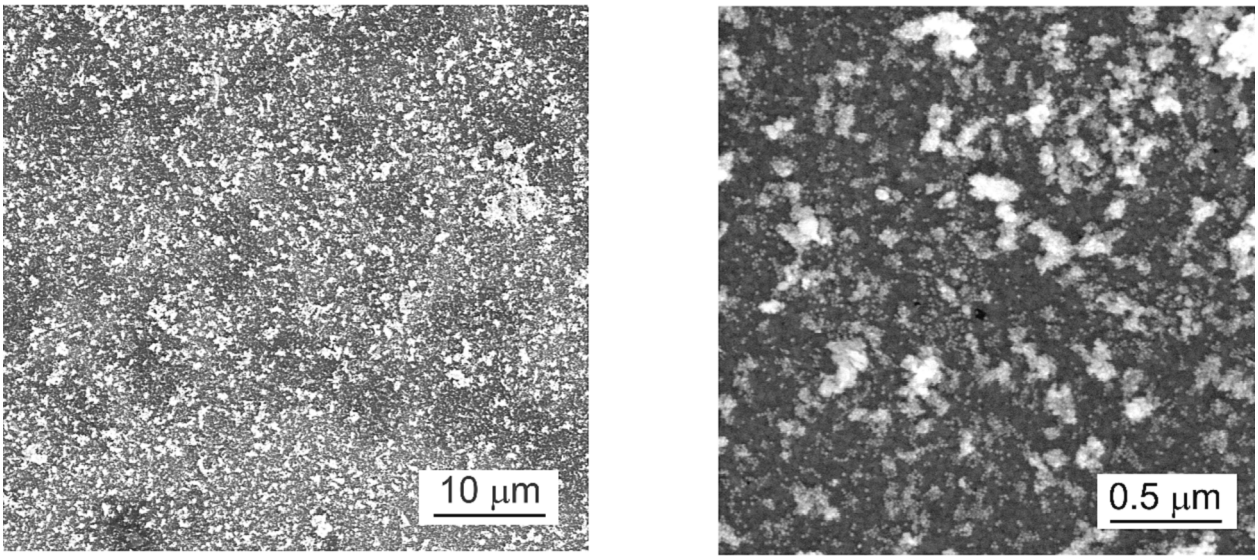

Fig. 2. SEM micrographs of the 2D-SERS sensor at different magnifications.

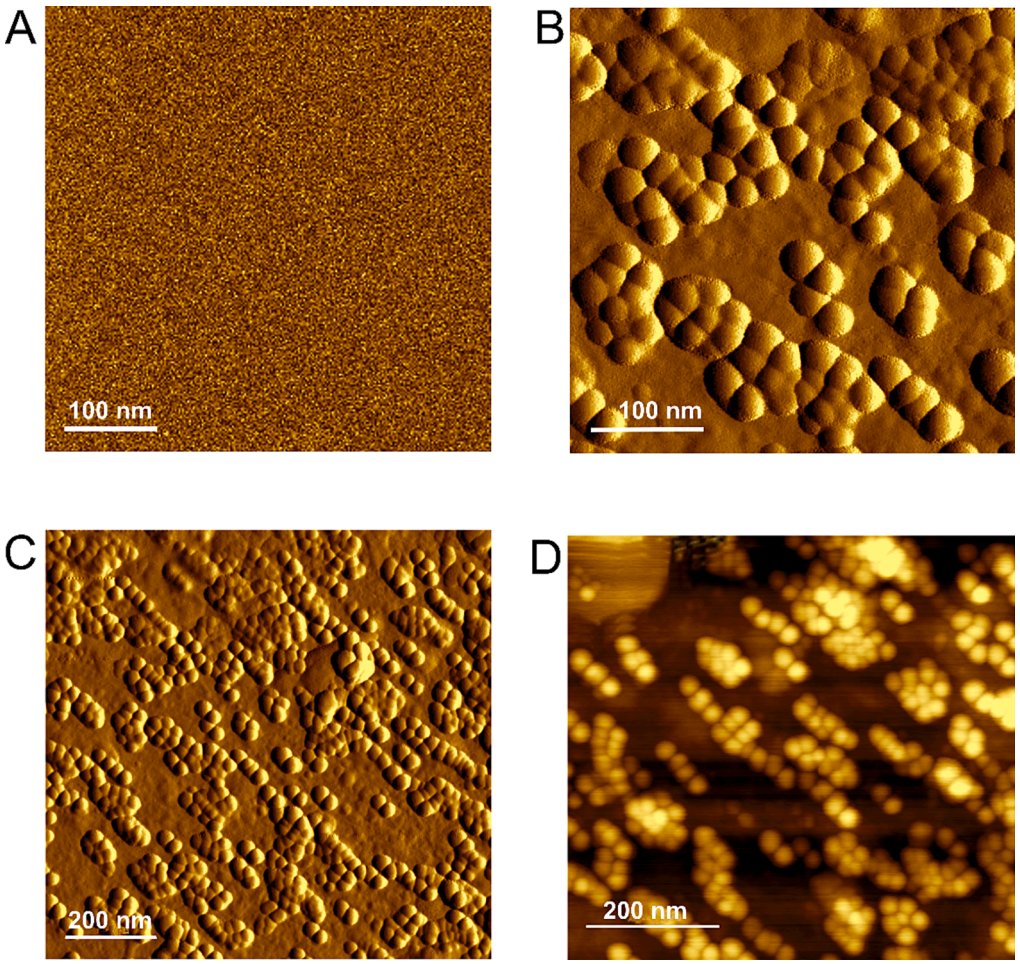

Fig. 3. AFM images of PGS@BDT (A) and PGS@BDT@AuNPs at different magnifications (B, C. D). Fig. 3C and 3D represent, respectively, the images collected in the magnitude mode and in the tip-height mode. The marker size is 100 nm for Fig. 3A – 3B and 200 nm for Fig. 3C – 3D.

anchoring of the gold nanoparticles was achieved by use of the BDT linker: one of the two thiol end-groups of the molecule is expected to react with the gold coating, while the other remains free for the successive grafting of the AuNPs This procedure should lead to a stable and homogenous distribution of the gold nanostructures on the PGS surface. [19,20].

The formation of a BDT Self Assembled Monolayer (SAM) was investigated by contact angle measurements. In fact, the pristine gold

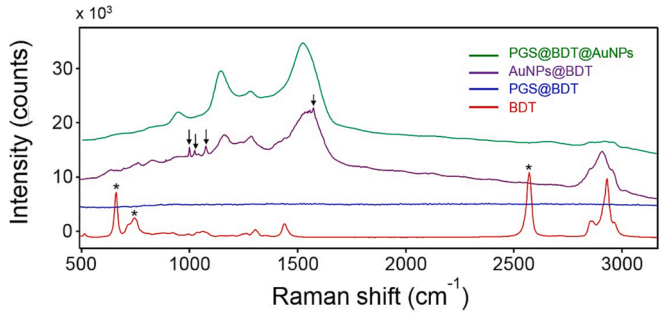

Fig. 4. Red trace: Raman spectrum of BDT (liquid). Blue trace: Raman spectrum of PGS@BDT. Violet trace: SERS spectrum of AuNPs@BDT deposited on aluminum substrate. Green trace: SERS spectrum of PGS@BDT@AuNPs. (For interpretation of the references to color in this figure legend, the reader is referred to the web version of this article.)

Table 1
Observed frequencies, calculated frequencies and normal mode assignments for the Raman spectrum of BDT (liquid). Potential Energy Distribution in Table S2, SM.

Observed [a] (cm^{-1})	Calculated [b] (cm^{-1})	Assignment [c]
2963 (m)	2995 (1.1)	$\nu_{op}(CH_2)_{2,5}$
2934 (vs)	2950 (0.5)	$\nu_{ip}(CH_2)_{2,5}$
2915 (s, sh)	2944 (1.0)	$\nu_{op}(CH_2)_{3,4}$
2860 (m)	2912 (1.8)	$\nu_{ip}(CH_2)_{3,4}$
2571 (vs)	2571 (<0.1)	ν(SH)
1440 (m)	1439 (0.07)	$\delta(CH_2)_{3,4}$
	1429 (0.8)	$\delta(CH_2)_{2,5}$
1351 (w)	1341 (0.7)	$\omega(CH_2)_{3,4}$
1305 (m)	1287 (1.4)	$\gamma(CH_2)_{3,4}$
1263 (w)	1251 (0.9)	$\omega(CH_2)_{2,5}$
1245 (w, sh)	1227 (1.4)	$\gamma(CH_2)_{2,5}$
1063 (w)	1078 (1.4)	HC
1037 (w)	1027 (1.0)	ν(C2C3)/ν(C4C5)
998 (w)	992 (0.6)	ν(C3C4)
810 (vw)	847 (4.5)	δ(HSC)
747 (m)	727 (2.7)	ν(CS)
662 (s)	690 (4.2)	δ(HSC)/ν(CS)

[a] : letters in round brackets indicate peak intensities: w = weak; m = medium; s = strong; v = very; sh = shoulder.

[b] : figures in round brackets are the % relative errors, $re = \frac{|\nu_{exp} - \nu_{calc}|}{\nu_{exp}} \bullet 100$.

[c] : Greek letters stand for: ν = stretching; δ = in-plane bending; γ = out-of-plane bending, twisting; ω = out-of-plane bending, wagging; subscripts to CH_2 denote the C labels as specified in the BDT structure reported in Fig. S4, SM; subscripts ip and op denote in-phase and out-of-phase vibrations, respectively; HC = highly coupled, i.e. a vibration involving the entire molecular structure.

surface is hydrophobic, while the introduction of polar SH groups on the surface is expected to increase the hydrophilicity. The average contact angle of plain PGS is 77°, which decreases down to 58° after BDT functionalization (see Fig. 1A – 1B).Further morphological analysis was performed by SEM and AFM measurements. Fig. 2 shows the SEM images of the 2D-SERS substrate at different magnifications.

Both the PGS and the PGS@BDT surfaces are featureless up to the highest magnification available for this technique (see Fig. 1A – 1B). Conversely, SEM analysis of the *2D-SERS* surface (PGS@BDT@AuNPs) clearly evidences the presence of the agglomerated nanoparticles. The distribution of these features across the surface appears to be homogeneous (Fig. 2, left), albeit a quantitative SIA cannot be attempted due to the highly irregular shape of the AuNPs domains. A more detailed analysis of the surface morphology has been performed by use of AFM, which, by virtue of its nanometric resolution, is capable of detecting the single nanoparticle. In Fig. 3A is reproduced a typical AFM image of the PSG. As for the SEM micrograph, a uniform background characteristic of a gold coated surface is observed.

The AuNPs are identified in Fig. 3B – D, representative of the PSG@BDT@AuNPs surface. These images highlight the uniform spherical shape and the size consistency of the AuNPs. No isolated nanospheres can be detected; the AuNPs are aggregated in clusters of varying size. A limited number of two- and three-particle clusters is occasionally observed. Typical dimeric structures display a lateral dimension of 60 nm, which reduces to 44 nm considering the lateral resolution (LR) of the AFM tip (LR = tip size = 8 nm). Thus, a single nanosphere, has a size of 22 nm according to AFM, a value in good agreement with the outcome of the SI analysis on TEM images (average particle size = 15 ± 2 nm).

The AFM images confirm the homogeneous distribution of AuNPs aggregates across the whole surface and highlight the vast amount of *hot-spots* present in the nanostructure, which are responsible for the remarkable SERS activity of the substrate.

The stability of the nanostructure is an essential requirement when the analyte transfer is done by drop-casting. Stability has been verified by surface analysis after consecutive washing cycles. AuNPs clusters are no longer visible on the PGS after the first washing/drying cycle while, due to the anchoring effect of BDT, the nanoscructure remains essentially invariant in the case of PGS@BDT@AuNPs after 3 cycles.

3.2. SERS spectroscopy

In Fig. 4 are compared the spectra of neat BDT (liquid) and of BDT adsorbed on different surfaces. In the 500 – 3200 cm^{-1} range the Raman spectrum of BDT (red trace in Fig. 4) displays several well resolved peaks. These have been assigned through a *QM*-based Normal coordinate analysis, whose details are reported in the Supplementary material (pages 4 – 7, *SM*). Observed and calculated peak frequencies, relative errors (*re*) and corresponding assignments are summarized in Table 1.

In general, the *ab-initio* simulation of the Raman spectrum is remarkably accurate ($\overline{re}$ = 1.4). The only two outliers are the modes involving the SH bond [δ(HSC) and δ(HSC)/ν(CS)] for which the *re's* are 4.5 and 4.2, respectively. The discrepancy is due to the influence of the medium, i.e., the self-interaction between SH groups occurring in the liquid phase. This effect is not accounted for by the adopted model (isolated molecule *in-vacuo),* which is otherwise adequate for our interpretative purposes. Ignoring the two outliers, the $\overline{re}$ reduces to 1.0 %, well within the predictive capabilities of DFT-based approaches [21] (between 1 and 3 %).

The relevant signals for the present analysis, denoted by asterisks in Fig. 4, are located at 2571 cm^{-1} (calculated at 2571 cm^{-1}), due to the SH stretching; at 810 cm^{-1} (calc. at 847 cm^{-1}) the HSC bending; at 747 cm^{-1} (calculated at 727 cm^{-1}) the CS stretching; and at 662 cm^{-1} (calculated at 690 cm^{-1}), due to a coupled δ(HSC)/ ν(CS) mode. The spectrum of PGS@BDT (blue trace in Fig. 4) is featureless which confirms that the flat gold surface is unable to induce any plasmonic enhancement. Conversely, significant SERS signaling is observed when BDT interacts with the gold nanoparticles. The violet pattern represents the SERS spectrum of an AuNPs colloidal solution functionalized by BDT and deposited onto an aluminum substrate. The SERS pattern is remarkably different from the spontaneous Raman spectrum of BDT. This is due to both chemical and orientational effects. As for the chemical effects, we observe the complete disappearance of the signals related to the SH group [2571 cm^{-1}, ν(SH); 810 cm^{-1}, δ(HSC); 662 cm^{-1}, δ(HSC)/ν(CS)]. This result confirms the reaction of the thiol group with the gold surface of the AuNPs, with formation of tiolate S–Au bonds. The absence of free SH groups suggests that both the thiol groups of BDT are chemisorbed on the nanoparticles. Thus, the linker has formed a cross-link between two AuNPs, generating a *hot-spot* between them. Since the plasmonic enhancement at this spot is much higher than that on an isolated nanoparticle, most of the SERS signal arises from these cross-links. SH signals are undetectable likely because of this effect, rather than for the complete consumption of thiol groups. The SERS spectrum exhibits prominent bands at 1285, 1540 and 2910 cm^{-1}. These

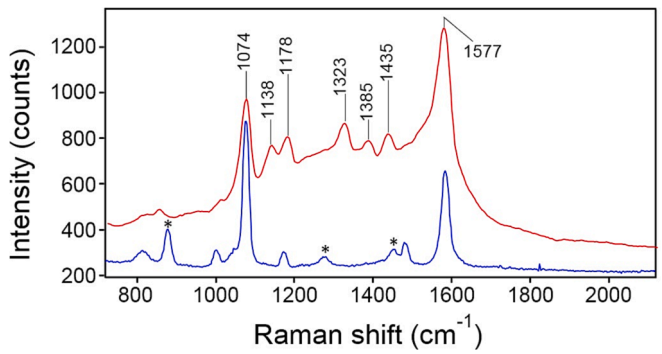

Fig. 5. Blue trace: SERS spectrum of AuNPs@pMA in a colloidal solution. Asterisks denote residual peaks of the co-solvent (ethanol). Red trace: SERS spectrum of pMA on PGS@BDT@AuNPs. (For interpretation of the references to color in this figure legend, the reader is referred to the web version of this article.)

can be tentatively associated to $\omega(CH_2)_{1,4}$, $\delta(CH_2)$ and $\nu(CH_2)$ vibrations. The remarkable blue-shift of the first two signals likely reflects the changing chemical environment of the methylene groups (from $–CH_2–SH$ to $–CH_2–SAu$). Two further features are observed at 947 cm^{-1} [ν(C2C3)] and at 1160 cm^{-1} (skeletal mode). Sharp, weak peaks denoted by arrows in Fig. 4, are likely due to residual impurities on the nanoparticle surface.

The green trace in Fig. 4 represents the SERS spectrum of BDT in the PGS@BDT@AuNPs substrate. The pattern is very close to that observed for the drop-cast colloidal solution (compare violet and green traces in Fig. 4), which demonstrates that anchoring of the AuNPs to the PGS substrate has occurred through the reaction of the linker. The main difference is the considerably reduced intensity of the $\nu(CH_2)$ band at 2910 cm^{-1} in the PGS@BDT@AuNPs spectrum, which is clearly due to orientational effects. Recalling that – according to the surface selection rules [22,23] – the maximum enhancement occurs when the polarizability tensor has the main components normal to the plasmonic surface, the above observation can be explained by assuming the CH_2 groups to lye almost parallel to the AuNPs surface. The geometry of this assembly is reasonable if one considers that BDT forms a SAM on the PGS with a specific orientation of the linker, which is likely locked-in when the nanoparticles react with the exposed SH group. Conversely, pre-reacted AuNPs@BDT can assume any orientation when deposited on a planar substrate.

To evaluate the SERS performances of the proposed 2D substrate we used pMA as molecular reporter due to its high reactivity towards the gold surface and the well-characterized inelastic scattering behaviour [24,25]. Co-localized SERS measurements were performed on PGS@BDT@AuNPs surfaces after functionalization with pMA.

In Fig. 5 the average SERS spectrum of pMA collected on a 10 x 10 μm map of the present 2D substrate is compared with the pMA SERS spectrum recorded on a colloidal solution of AuNPs. The two patterns display common peaks at 1074, 1178 and 1577 cm^{-1}, which confirm the chemisorption of pMA on the nanoparticle surface. In fact, the preliminary anchoring of the AuNPs with BDT is expected to occur in the bottom area of the nanoparticle, leaving the rest of the surface available for further reaction. Several other peaks not present in the SERS spectrum of the colloid emerge at 1138, 1385 and 1435 cm^{-1}. These are due to dimeric azo-species formed by a photochemically triggered reaction [18,26]. It has been demonstrated that this reaction can only occur in the presence of a suitable concentration of *hot-spots* which increase substantially the plasmonic effect [18]. This situation occurs in the present 2D substrate (see AFM images in Fig. 3), but not in the diluted colloidal solution.

The spectra reported in Fig. 5 allow us to estimate the Enhancement Factor, *EF* – the main figure of merit for SERS substrates – according to the methods described in 2.2, Experimental Section. For both substrates, full coverage of the reactive surface was assumed. The estimated *EF* values were 5.4×10^5 and 2.60×10^8, for the colloid and the 2D substrate, respectively. The colloidal solution exhibits an *EF* value consistent with previous literature data [18]; the planar substrate displays an *EF* increase of about three orders of magnitude, making it suitable for hypersensitive analytical applications. The superior SERS efficiency of the proposed sensor is related to the high concentration and stability of *hot-spots*, that are realized with our bottom-up nanoassembly protocol. In a separate experiment, we verified that BDT anchoring is essential for optimum SERS performances of the sensor in terms of both intensity and stability. In fact, without the BDT pre-treatment, the AuNPs deposited on the PGS are completely washed out by the pMA/ethanol analytical solution and no SERS activity is observed (see Fig. S4A-B, *SM*).

An equally relevant figure of merit for a planar SERS sensor, especially when quantitative analysis is concerned, is the response homogeneity of the sensing surface. This feature has been investigated by co-localized Raman imaging (see Fig. 6, where the color map is reconstructed by reporting the intensity of the 1074 cm^{-1} peak in the spatial coordinate frame). The co-localized map in Fig. 6 highlights a substantial SERS activity in the whole sampled area, spanning from 10,000 to 15,000 counts/cm in terms of peak area, or from 1.6 x 10^8 to 2.4 x 10^8 in terms of *EF*. A more complete statistical analysis of the SERS

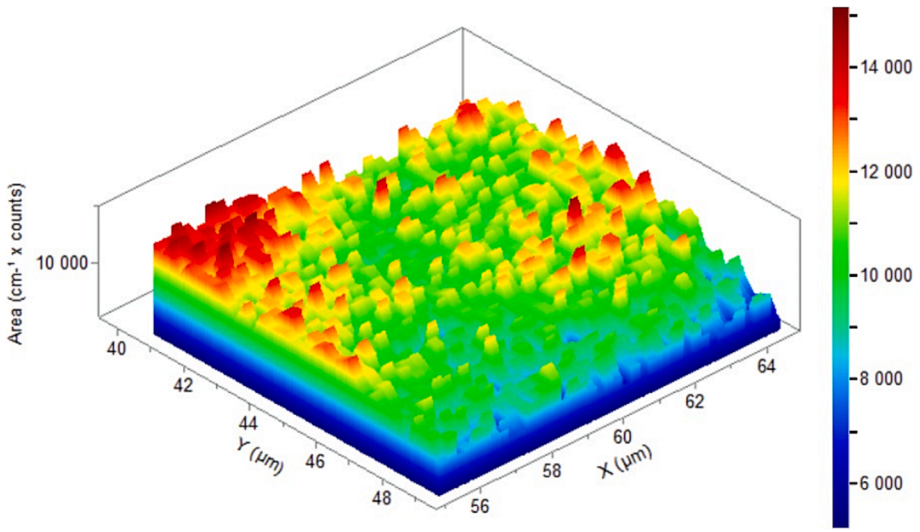

Fig. 6. Co-localized SERS map of pMA on PGS@BDT@AuNPs, reconstructed by considering the area of the 1074 cm^{-1} peak.

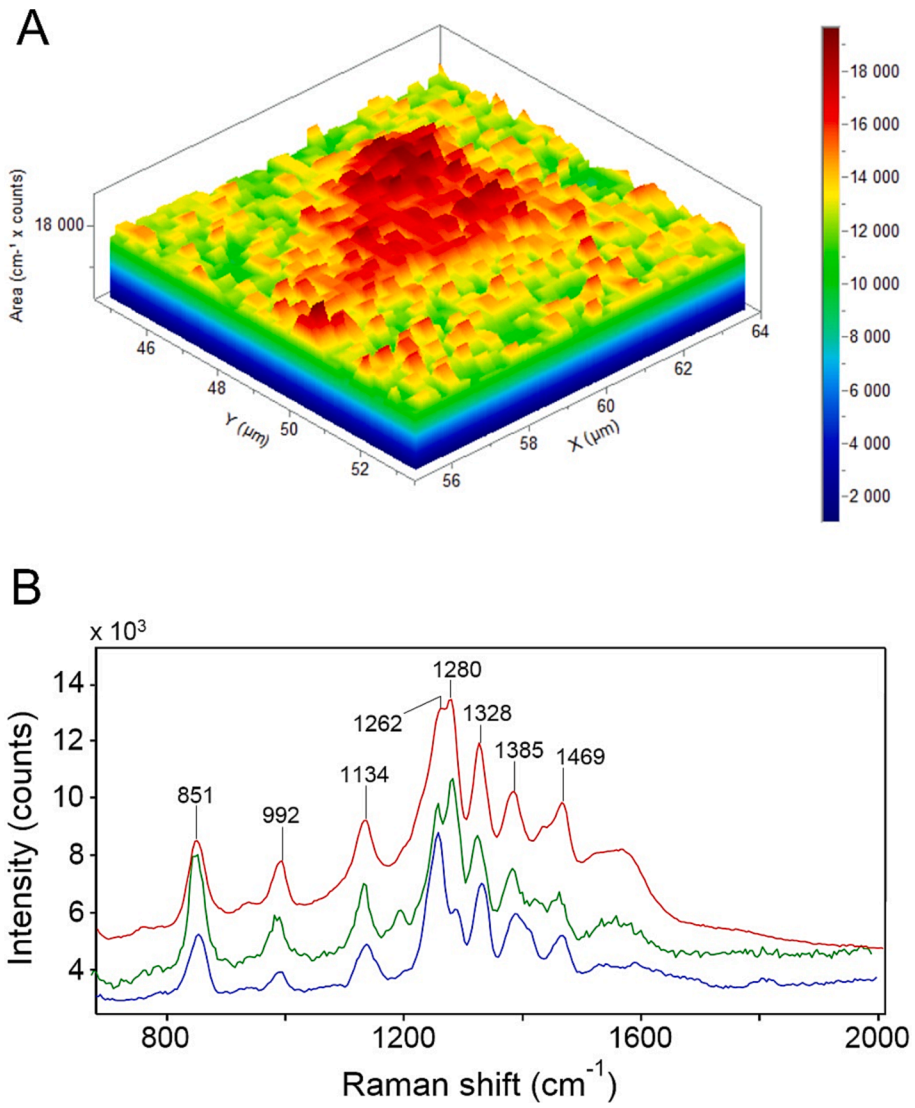

Fig. 7. A) Co-localized SERS map of a 20 μM solution of 6-MP on PGS@BDT@AuNPs, reconstructed by considering the peak at 851 cm^{-1}. B) Blue trace: SERS spectrum of AuNPs@6-MP in a colloidal solution (50 μM). Green trace: SERS spectrum of AuNPs@6-MP (50 μM) on aluminum substrate. Red trace: SERS spectrum of 6-MP on PGS@BDT@AuNPs (average spectrum from the map in Fig. 7A).. (For interpretation of the references to color in this figure legend, the reader is referred to the web version of this article.)

performance was carried out on six maps collected in several places of the 2D-sensor. The whole hyperspectral data set comprises 6000 spectra: the average peak intensity is (7.0 ± 0.9) x 10^3 counts/cm; the average Enhancement Factor, $\overline{EF}$, is (2.3 ± 0.3) x 10^8. The two figures of merit derived from our statistical analysis, i.e., $\overline{EF}$ and its standard deviation, σ, demonstrate that the proposed nanoparticle assembly can be suitable for analytical purposes in terms of sensitivity, accuracy and reproducibility.

3.3. Analytical application

The 2D-SERS substrate was tested as sensing platform for Therapeutic Drug Monitoring (TDM). In particular, we developed a protocol for the quantitative detection of the anticancer drug 6-MP [11]. The assay was performed by dropping a 100 μL aqueous solutions of 6-MP at different concentrations in the range 5 – 20 μM. After drying, we performed co-localized measurements on several areas of the sensing surface: a typical Raman image is reported in Fig. 7A, while in Fig. 7B the average spectrum of the map is compared with the 6-MP SERS spectra in a plain AuNPs casting and in a colloidal solution.

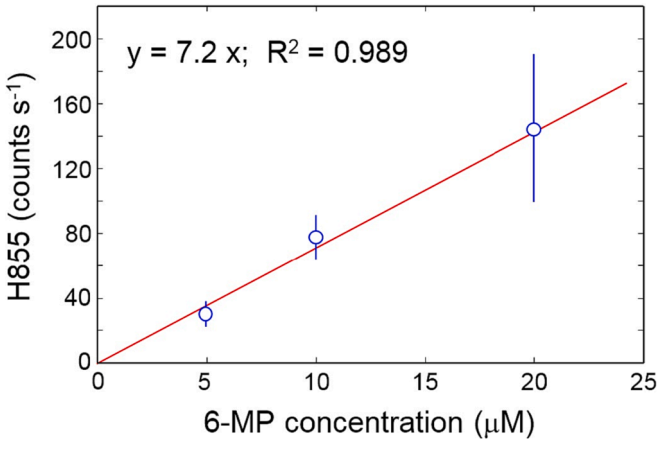

Fig. 8. Calibration curve for the quantitative analysis of 6-MP by SERS: intensity of the 6-MP signal at 852 cm^{-1} as a function of the analyte concentration.

The spectrum of the present 2D-substrate is essentially coincident with the two reference spectra, which confirms the chemisorption of the analyte on the plasmonic surface and the absence of significant interference by the BDT linker.

Fig. 8 displays the intensity vs concentration diagram relative to the 6-MP peak at 852 cm^{-1}. The explored concentration range (5–20 μM) is that of clinical interest [14,15]. A satisfactory linear correlation crossing the origin is observed, represented by the equation:

$$I_{852}\left(counts{\cdot}s^{-1}\right) = 7.2{\cdot}C_{6MP}(\mu M)$$

where I_{852} is the intensity (height) of the analytical peak normalized for exposure time, and C_{6MP} is the analyte concentration in μmol/L. The correlation coefficient, $R^2 = 0.989$ confirms the suitability of the present assaying platform for TDM applications. The error bars in Fig. 8 represent the data scattering of the peak intensity around the mean, calculated for at least four co-localized SERS maps on PGS@BDT@AuNPs. The relative standard deviation, which reflects the uniformity of the response function, is appropriate at 5 and 10 μM (12.7 and 17.5 %, respectively), but increases significantly up to 33.0 % at 20 μM, suggesting a decay of accuracy when approaching the upper limit of the working range. The origin of this effect is currently under investigation.

4. Conclusions

The present contribution describes the fabrication and characterization of a SERS sensor based on gold nanospheres deposited onto a suitably functionalized metal surface. To achieve a homogeneous distribution and a long-term stability of the deposition, a dithiol linker has been reacted with the substrate before the drop-casting procedure. A stable anchoring of the AuNPs onto the sensing surface has been confirmed by TEM, AFM and SERS measurements. The performance of the 2D sensor has been evaluated in terms of the SERS Enhancement Factor, which provided a value of $2.3{\times}10^8$, well suited for hypersensitive analytical applications. As for a real-world application, the proposed sensor has been tested for the Therapeutic Drug Monitoring of the anticancer drug 6-MP. Promising results have been achieved in terms of both sensitivity and accuracy in a concentration range of clinical interest.

Declaration of Competing Interest

The authors declare that they have no known competing financial interests or personal relationships that could have appeared to influence the work reported in this paper.

Data availability

Data will be made available on request.

Appendix A. Supplementary data

Supplementary data to this article can be found online at https://doi.org/10.1016/j.saa.2024.123983.

References

[1] E. Le Ru, P. Etchegoin, Principles of surface-enhanced raman spectroscopy and related plasmonic effects, Elsevier, 2008.
[2] S. Pang, T. Yang, L. He, Review of surface enhanced Raman spectroscopic (SERS) detection of synthetic chemical pesticides, TrAC Trends Anal. Chem. 85 (2016) 73–82, https://doi.org/10.1016/j.trac.2016.06.017.
[3] S. Schlucker, Surface enhanced raman spectroscopy. Analytical, biophysical and life science applications, John Wiley & Sons, 2011.
[4] T. Vo-Dinh, et al., SERS nanosensors and nanoreporters: Golden opportunities in biomedical applications, WIREs Nanomed. Nanobiotechnol. 7 (2015) 17–33, https://doi.org/10.1002/wnan.1283.
[5] S. Fornasaro, et al., surface enhanced raman spectroscopy for quantitative analysis: Results of a large-scale european multi-instrument interlaboratory study, Anal Chem 92 (2020) 4053–4064, https://doi.org/10.1021/acs.analchem.9b05658.
[6] S.E.J. Bell, et al., Towards reliable and quantitative surface-enhanced raman scattering (SERS): From key parameters to good analytical practice, Angew. Chem. Int. Ed. 59 (2020) 5454–5462, https://doi.org/10.1002/anie.201908154.
[7] J. Son, et al., Toward quantitative surface-enhanced raman scattering with plasmonic nanoparticles: Multiscale view on heterogeneities in particle morphology, surface modification, interface, and analytical protocols, J Am Chem Soc 144 (2022) 22337–22351, https://doi.org/10.1021/jacs.2c05950.
[8] V.S. Vendamani, S.V.S.N. Rao, A.P. Pathak, V.R. Soma, Silicon nanostructures for molecular sensing: A review, ACS Applied Nano Materials 5 (2022) 4550–4582, https://doi.org/10.1021/acsanm.1c04569.
[9] L. Lennard, The clinical pharmacology of 6-mercaptopurine, Eur J Clin Pharmacol 43 (1992) 329–339, https://doi.org/10.1007/bf02220605.
[10] J.S. Kang, M.H. Lee, Overview of therapeutic drug monitoring, Korean J Intern Med 24 (2009) 1–10, https://doi.org/10.3904/kjim.2009.24.1.1.
[11] M.V. Relling, M.L. Hancock, J.M. Boyett, C.-H. Pui, W.E. Evans, Prognostic Importance of 6-Mercaptopurine Dose Intensity in Acute Lymphoblastic Leukemia, Blood 93 (1999) 2817–2823, https://doi.org/10.1182/blood.V93.9.2817.
[12] R.H. Larsen, et al., Pharmacokinetics of tablet and liquid formulations of oral 6-mercaptopurine in children with acute lymphoblastic leukemia, Cancer Chemother. Pharmacol. 86 (2020) 25–32, https://doi.org/10.1007/s00280-020-04097-x.
[13] L. Alnaim, Therapeutic drug monitoring of cancer chemotherapy, J. Oncol. Pharm. Pract. 13 (2007) 207–221, https://doi.org/10.1177/1078155207081133.
[14] E. Jacqz-Aigrain, et al., Pharmacokinetics and distribution of 6-mercaptopurine administered intravenously in children with lymphoblastic leukaemia, Eur. J. Clin. Pharmacol. 53 (1997) 71–74.
[15] M. Pannico, P. Musto, SERS spectroscopy for the therapeutic drug monitoring of the anticancer drug 6-Mercaptopurine: Molecular and kinetic studies, Appl. Surf. Sci. 539 (2021) 148225, https://doi.org/10.1016/j.apsusc.2020.148225.
[16] M. Pannico, P. Musto, pH activated colloidal Nanospheres: A viable sensing platform for the Therapeutic Drug Monitoring of the anticancer Drug 6-Mercaptopurine, Appl. Surf. Sci. 570 (2021) 151232, https://doi.org/10.1016/j.apsusc.2021.151232.
[17] M. Pannico, A. Calarco, G. Peluso, P. Musto, Functionalized gold nanoparticles as biosensors for monitoring cellular uptake and localization in normal and tumor prostatic cells, Biosensors 8 (2018) 87.
[18] M. Pannico, et al., Direct printing of gold nanospheres from colloidal solutions by pyro-electrohydrodynamic jet allows hypersensitive SERS sensing, Appl. Surf. Sci. 531 (2020) 147393.
[19] E. Azzam, et al., Fabrication of a surface plasmon resonance biosensor based on gold nanoparticles chemisorbed onto a 1, 10-decanedithiol self-assembled monolayer, Thin Solid Films 518 (2009) 387–391.
[20] O. Kvítek, R. Hendrych, Z. Kolská, V. Švorčík, Grafting of gold nanoparticles on glass using sputtered gold interlayers, J. Chem. 2014 (2014).
[21] S.F. Sousa, P.A. Fernandes, M.J. Ramos, General performance of density functionals, Chem. A Eur. J. 111 (2007) 10439–10452, https://doi.org/10.1021/jp0734474.
[22] R. Aroca, Surface-enhanced vibrational spectroscopy, John Wiley & Sons, England, 2006.
[23] X. Gao, J.P. Davies, M.J. Weaver, A test of surface selection rules for surface-enhanced raman scattering: The orientation of adsorbed benzene and monosubstituted benzenes on gold, J. Phys. Chem. 94 (1990) 6858–6864.
[24] N. Mohri, S. Matsushita, M. Inoue, K. Yoshikawa, Desorption of 4-aminobenzene-thiol bound to a gold surface, Langmuir 14 (1998) 2343–2347.
[25] A. Gopinath, S.V. Boriskina, B.M. Reinhard, L. Dal Negro, Deterministic aperiodic arrays of metal nanoparticles for surface-enhanced Raman scattering (SERS), Opt. Express 17 (2009) 3741–3753.
[26] Y.-F. Huang, et al., Surface-enhanced Raman spectroscopic study of p-aminothiophenol, PCCP 14 (2012) 8485–8497.